AD-A181 002 CALCULATION OF THE STABILITY OF HEATED BOUNDARY LAYERS USING THE COMPOUND..(U) ADMIRALTY RESEARCH ESTABLISHMENT TEDDINGTON (ENGLAND) D J ATKINS DEC 86 1/1

UNCLASSIFIED ARE-TM-(UHA)-86514 DRIC-BR-101905 F/G 20/13 NL

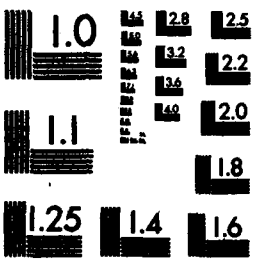

CALCULATION OF THE STABILITY OF HEATED BOUNDARY LAYERS USING THE COMPOUND MATRIX METHOD

by

D J ATKINS

Summary

A fourth-order Orr-Sommerfeld eigenvalue solver for heated boundary layers ~~developed by BMT Ltd~~ has been implemented on the VAX-11/785 computer ~~at ARE(Teddington)~~. The solver is based on the compound matrix method and the effects of heating are limited to mean viscosity variation across the boundary layer. Some test computations have been carried out on flat plates with uniform wall temperature. For small overheat, the results agree with those previously published using other methods, but for large overheat, there are some minor differences. The calculation procedure requires a large number of integration steps across the boundary layer to obtain accurate eigenvalues, but is relatively insensitive to other physical and numerical parameters. A few computations have been carried out using a full sixth-order model ~~, also developed by BMT Ltd.~~, which takes into account fluctuations in all the fluid properties. It is concluded that the fourth-order method can be incorporated into an axisymmetric body calculation procedure. (Great Britain)

52 pages
15 figures

ARE (Teddington)
Queen's Road
Teddington Middx TW11 0LN

December 1986

C O N T E N T S

LIST OF SYMBOLS

C_p	Specific heat capacity (J $kg^{-1}K^{-1}$)
$\bar{c}$	Dimensionless complex wavespeed (= $\omega/\alpha u_e$)
f	Dimensionless stream function, defined by equation (A12)
k	Thermal conductivity (W $m^{-1}K^{-1}$)
R	Displacement thickness Reynolds number (= $u_e\delta^*/\nu_\infty$)
T	Absolute temperature (K)
u	Velocity component in x-direction (m s^{-1})
$\bar{u}$	Dimensionless velocity (= u/u_e)
v	Velocity component in y-direction (m s^{-1})
x	Streamwise co-ordinate (m)
y	Normal co-ordinate (m)
α	Complex wavenumber
$\bar{\alpha}$	Dimensionless complex wavenumber (= $\alpha\delta^*$)
δ^*	Boundary-layer displacement thickness, defined by equation (1)
η	Transformed normal co-ordinate, defined by equation (A9)
μ	Dynamic viscosity (N s m^{-2})
$\bar{\mu}$	Dimensionless viscosity (= μ/μ_∞)
ν	Kinematic viscosity (m^2s^{-1})
ξ	Transformed boundary-layer streamwise co-ordinate
ρ	Density (kg m^{-3})
ϕ	Amplitude of disturbance stream function
ω	Angular frequency
$\bar{\omega}$	Dimensionless angular frequency (= $\omega\delta^*/u_e$)

Subscripts

e	Value at outer edge of boundary layer
i	Imaginary part of complex quantity
r	Real part of complex quantity
w	Value at plate surface
∞	Freestream value

INTRODUCTION

The drag of an underwater vehicle can be substantially reduced by delaying transition from laminar to turbulent flow in the boundary layer. This results in higher speed for a given power input or a reduced power input to achieve the same speed. One way of delaying transition is by heating the surface. The viscosity of water decreases with temperature, and this phenomenon combined with surface heating results in a more stable boundary layer.

The prediction of the transition location on a heated body can be carried out by adapting the well-established procedures for an unheated body based on linear stability theory [1]. Starting at the nose and working downstream, laminar boundary-layer mean-flow profiles are calculated at several positions on the body surface. For each set of profiles, the spatial growth rates of two-dimensional disturbances are calculated at several frequencies by obtaining eigenvalues of the fourth-order Orr-Sommerfeld equation. The growth rates at a specific frequency are then integrated along the body surface and the location where the total amplification ratio is e^n (with n usually having the value 9) is calculated. The most forward of these locations is the predicted transition location. Although the method assumes parallel mean flow and two-dimensional disturbances, it has been widely verified experimentally.

The objective of the present investigation is to validate a fourth-order eigenvalue solver developed by BMT Ltd based on the compound matrix method. The heated flat plate with uniform wall temperature was used as a test case, since the partial differential equations describing the mean flow reduce to ordinary differential equations which can be solved very accurately and eigenvalue computations can be compared with previously published results. A few numerical results have been obtained using a sixth-order system of equations which includes viscosity, temperature and density fluctuations and buoyancy effects.

2. THEORY

The equations of the mean flow over a flat plate with uniform temperature are derived and stated in Appendix A (equations (A22) and (A23)) along with the boundary conditions ((A18), (A19) and (A21)). The solution of these equations gives profiles of dimensionless velocity and temperature and their first and second derivatives. The only physical input required is a knowledge of the fluid properties (density, viscosity, specific heat capacity and thermal conductivity), which are assumed to vary only with temperature. Two sets of expressions for these quantities have been used, proposed by Lowell & Reshotko [2] and Kaups & Smith [3]. Full details are included in Appendix B.

The modified Orr-Sommerfeld equation requires as input the dimensionless velocity profile u/u_e and its second derivative, expressed as functions of the displacement thickness unit y/δ^*, where δ^* represents the usual boundary-layer displacement thickness, given by

$$\delta^* = \int_0^\infty \left\{1 - \frac{\rho\ u}{\rho_\infty\ u_e}\right\} dy \qquad (1)$$

It also requires the dimensionless viscosity μ/μ_e and its first and second derivatives (which depend on temperature) expressed as functions of y/δ^*. However, the velocity and temperature profiles and their derivatives output by the mean flow calculation are functions of η, the compressible scaling parameter (equation (A9), Appendix A). To convert the mean flow profiles to a form suitable for input to the eigenvalue calculation, a numerical procedure and FORTRAN-77 computer program (known as NMIAL514) were written and supplied by NMI Ltd (now BMT Ltd) [4]. In a typical boundary-layer calculation, 80 to 100 points are normally sufficient to determine the mean velocity and temperature profiles, whereas the number of data points (or integration steps) required for accurate eigenvalue calculation is much larger (typically 800). Program NMIAL514 also carries out the required interpolation to achieve this using a cubic polynomial method. As originally supplied, the program reads in profiles at 81 input points and interpolates them to 801 output points (equivalent to 800 integration steps), but it has been modified so that both these numbers can be varied.

The eigenvalue calculation method solves the Orr-Sommerfeld equation

$$(\bar{u} - \bar{c})(\phi'' - \bar{\alpha}^2\,\phi) - \bar{u}''\,\phi + \frac{i}{\bar{\alpha}\,R}\left\{\bar{\mu}\,(\phi'''' - 2\,\bar{\alpha}^2\,\phi'' + \bar{\alpha}^4\,\phi)\right.$$

$$\left. + 2\,\bar{\mu}'\,(\phi''' - \bar{\alpha}^2\,\phi') + \bar{\mu}''\,(\phi'' + \bar{\alpha}^2\,\phi)\right\} = 0 \qquad (2)$$

which has been modified to include viscosity variations in the mean flow. The mean flow is assumed to be parallel and the stream function representing a single disturbance is assumed to be of the form

$$\psi\,(x, y, t) = \phi(y)\,\exp\{i\bar{\alpha}(x-ct)\} \qquad (3)$$

The boundary conditions are

$$\phi(0) = \phi'(0) = \phi(\infty) = \phi'(\infty) = 0 \qquad (4)$$

A numerical procedure and computer program (known as NMIHE40S) has been supplied by NMI Ltd. [4] based on the compound matrix method [5]. This particular method was used to avoid any numerical problems caused by the fact that the Orr-Sommerfeld equation is stiff. The program was written in an interactive

form, but it has since been modified to allow for automatic calculation of eigenvalues. The eigenvalue relation has the form

$$F(\bar{\alpha}, \bar{\omega}, R) = 0 \quad \text{with} \quad \bar{\alpha} = \bar{\alpha}_r + \bar{\alpha}_i \quad \text{and} \quad \bar{\omega} = \bar{\omega}_r + \bar{\omega}_i \qquad (5)$$

There are three modes of operation. Mode 0 gives temporal instabilities. $\bar{\alpha}_r$ and $\bar{\alpha}_i$ are specified (with $\bar{\alpha}_i = 0$) and the program calculates $\bar{\omega}_r$ and $\bar{\omega}_i$. A positive value of $\bar{\omega}_i$ indicates an unstable mode. Mode 1 (spatial instability) is where $\bar{\omega}_r$ and $\bar{\omega}_i$ are specified ($\bar{\omega}_i = 0$) and $\bar{\alpha}_r$ and $\bar{\alpha}_i$ are calculated. Mode 2 (also spatial instability) is where $\bar{\alpha}_r$ and $\bar{\omega}_i = 0$ are specified and $\bar{\alpha}_i$ and $\bar{\omega}_r$ are calculated. A negative value of $\bar{\alpha}_i$ in modes 1 and 2 indicates an unstable mode. The spatial instability modes are of greatest practical interest and most of the eigenvalue computations described in Section 3 are using these modes.

BMT Ltd. have also supplied two further computer programs known as BMTMF2 and BMTST6 [6], which are similar to NMIAL514 and NMIHE40S but deal with the sixth-order system derived by Lowell & Reshotko [2], which includes fluctuations in all the flow variables. They found that buoyancy effects are negligible. The programs only deal with the temporal instability case and a few numerical results are presented in Appendix E.

3. NUMERICAL RESULTS

This section describes test computations on heated and unheated flat plates with constant wall temperature. The cases chosen were those used by Lowell & Reshotko [2], corresponding to an ambient temperature of approximately 15.6°C (60°F) and wall temperatures of approximately 15.6°C (60°F), 32.2°C (90°F), 65.6°C (150°F) and 93.3°C (200°F). The Reynolds number range was from 400 to 20,000, based on the displacement thickness δ^*. This is typical of the range required in transition calculations, since δ^* is generally much smaller than other characteristic length scales, such as body length or diameter.

Full details of the mean flow computations are presented in Appendix C. The mean flow profiles were converted to profiles of dimensionless velocity and its second derivative (expressed as functions of y/δ^*) using a modified version of program NMIAL514. The converted profiles were input to a modified version of program NMIHE40S to calculate the eigenvalues.

Lowell & Reshotko [2] presented the results of their eigenvalue calculations in terms of neutral stability curves, which are contour plots of curves of $\bar{\alpha}_i = 0$ as a function of Reynolds number R and $\bar{\alpha}_r$. To obtain comparisons with their work,

similar plots were obtained using a procedure described in Appendix D.

(a) Unheated plates

Some tabular comparisons of unheated flat plate eigenvalues are described in Appendix D. These show the compound matrix method to be both well-conditioned numerically (only single precision using 32-bit arithmetic is required) and capable of giving eigenvalues to high accuracy. Figure 1 shows the effect of the number of integration steps on the neutral stability curve. The results show that 800 integration steps are required to obtain accurate eigenvalues over the whole range of $\bar{\alpha}_r$ and R. The results for 800 steps agree with those of Lowell & Reshotko. The eigenvalue calculation at high values of $\bar{\alpha}_r$ R appears to be sensitive to the number of steps. At these values, it is also particularly sensitive to the initial guesses for $\bar{\alpha}_i$ and $\bar{\omega}$ (see Appendix D).

An alternative eigenvalue solver for the unheated case, supplied by ARE (Portland), was also tested. This was originally written by NPL [7], and uses a matrix method with finite-difference approximations to the derivatives of the Orr-Sommerfeld equation. The results using this method are presented as Figure 2. There was less variation in the solutions obtained using 100, 200 and 400 steps than with the compound matrix method, but at 100 and 200 steps the minimum critical Reynolds numbers were calculated to be 557 and 528 as opposed to the accepted value of 519 [8]. The solution for 400 steps using this method and all the compound matrix solutions for 200 steps and above gave answers within 1% of the accepted value. However, the accuracy of the NPL method may still be satisfactory in engineering calculations of flow transition. At large numbers of steps (greater than about 400), the method appears to suffer from ill-conditioning. It is implemented in double precision (64-bit arithmetric).

The effect of varying the freestream boundary is shown in Figure 3. Using 800 integration steps, values for η_e of 10.0, 7.5 and 5.0 were tried. The results for 10.0 and 7.5 were almost identical, and those for 5.0 were slightly different.

(b) Heated plates

Some numerical results are presented in tabular form and discussed in Appendix E. The effect of the number of integration steps on the neutral stability curve was examined for the cases of wall temperature 32.2°C (90°F) and 93.3°C (200°F) with an ambient temperature of 15.6°C (60°F). The freestream boundary in the mean flow calculation was at $\eta = 10$ and the fluid property relations were those of Lowell & Reshotko [2]. In the former case (Figure 4),

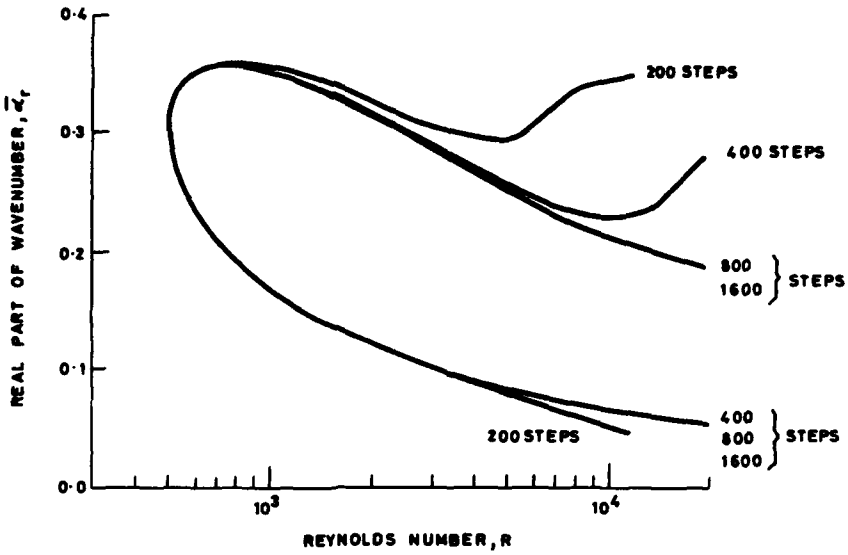

FIG. 1 EFFECT OF NUMBER OF INTEGRATION STEPS ON NEUTRAL STABILITY CURVE CALCULATED USING COMPOUND MATRIX METHOD (UNHEATED PLATE)

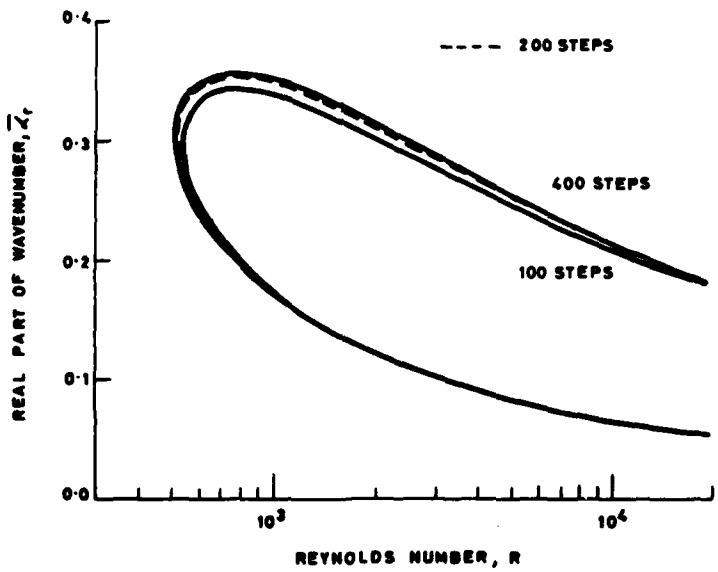

FIG. 2 EFFECT OF NUMBER OF INTEGRATION STEPS ON NEUTRAL STABILITY CURVE CALCULATED USING NPL METHOD [7] (UNHEATED PLATE)

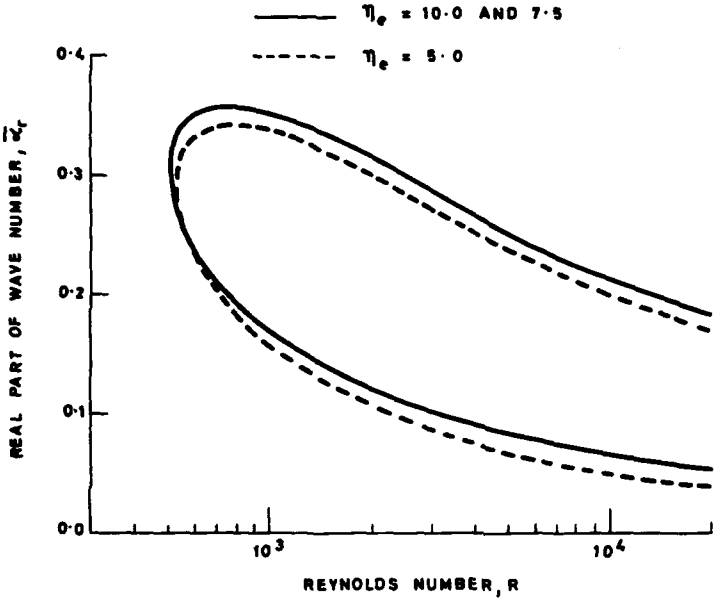

FIG. 3 EFFECT OF FREESTREAM BOUNDARY ON NEUTRAL STABILITY CURVE (UNHEATED PLATE)

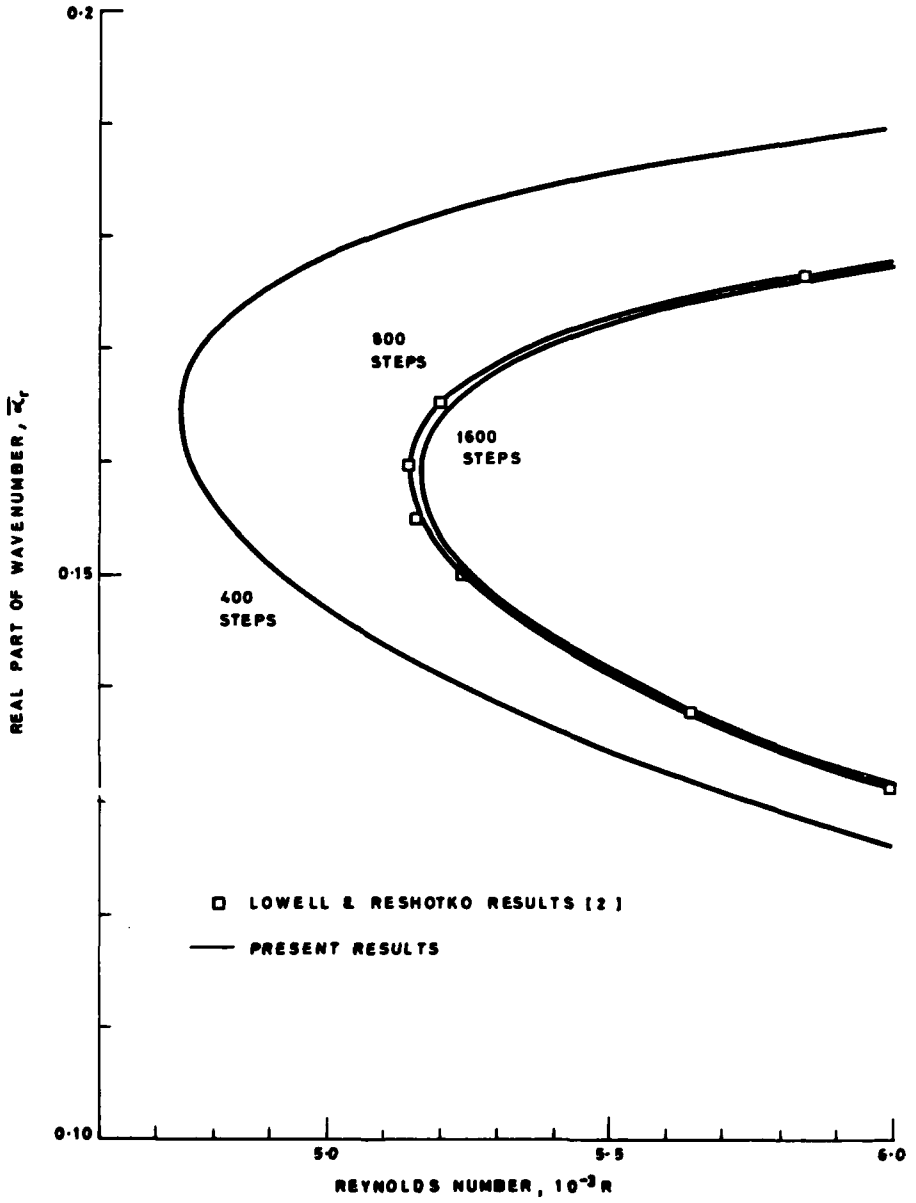

FIG. 4 EFFECT OF NUMBER OF INTEGRATION STEPS ON NEUTRAL STABILITY CURVE OF HEATED PLATE
(T_{∞} = 15·6°C(60°F) T_w = 32·2°C (90°F))

800 integration steps are sufficient for practical calculation purposes, but in the latter case (Figure 5), at least 1600 steps are required. Figures 4 and 5 also show the numerical results of Lowell & Reshotko, who used an orthonormalization method. At the lower temperature difference, their results agree well with those using the compound matrix method with 800 integration steps. At the higher temperature difference, however, their results lie somewhere between those using 800 and 1600 steps. According to Reference 2, they used 1000 steps, which the present results suggest may not be enough. Their values of dimensionless wall shear-stress and temperature gradient agree with those in the present investigation (see Appendix C). The effect of changing the freestream boundary is shown in Figure 6 corresponding to the largest overheat; the results are similar to those for the unheated case mentioned above.

The effects of using different fluid property relations are shown in Figures 7 and 8, corresponding to small and large overheats respectively. Two sets of relations were tried, those used by Lowell & Reshotko [2] and those of Kaups & Smith [3] (for details, see Appendix B). The assumption of constant density was tried in the Lowell & Reshotko formulae and made very little difference to the calculated eigenvalues.

Figure 9 shows the effect of different wall temperatures on the neutral stability curve. These results were obtained using the Kaups & Smith fluid property relations (for comparison with those in Reference 2), with variable density. The mean flows were computed using an accurate fourth-order method (Method 2, Appendix C). Similar plots were obtained using different fluid property relations (including one case with constant density) and the results (when compared graphically) were almost indistinguishable from those in Figure 9. It should be noted that the Reynolds number is on a logarithmic scale. Further results where the mean flows were computed using a second-order finite-difference method (Method 4, Appendix C) were also very similar. The results obtained by Lowell & Reshotko are also shown. A plot of minimum critical Reynolds number against overheat ($T_w - T_\infty$) is presented as Figure 10. This shows the data collected by Lowell & Reshotko, to which the present numerical results have been added. The optimum overheat is seen to be about 40°C.

A few numerical results were obtained using the sixth-order formulation [6]. These are limited to the temporal instability case (Mode 0) with a wall temperature of 32.2°C (90°F) and are described in Appendix E. Comparison with the fourth-order formulation shows differences in eigenvalues which are nontrivial but small. The resulting neutral stability curves (Figure 11) correspond with those of Lowell & Reshotko [2]. It should be noted that, on the neutral stability curves only, the spatial and temporal eigenvalues coincide.

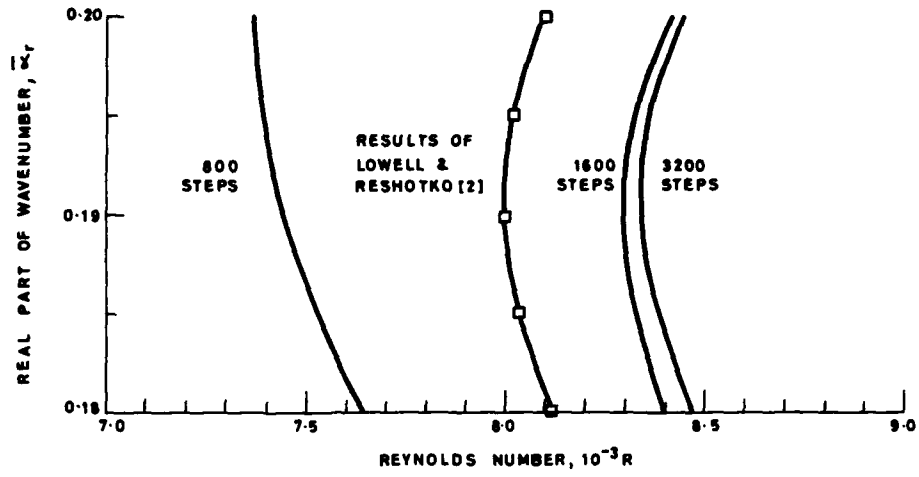

FIG. 5 EFFECT OF NUMBER OF INTEGRATION STEPS ON NEUTRAL STABILITY CURVE OF HEATED PLATE (T_∞ = 15·6°C (60°F), T_w = 93·3°C (200°F))

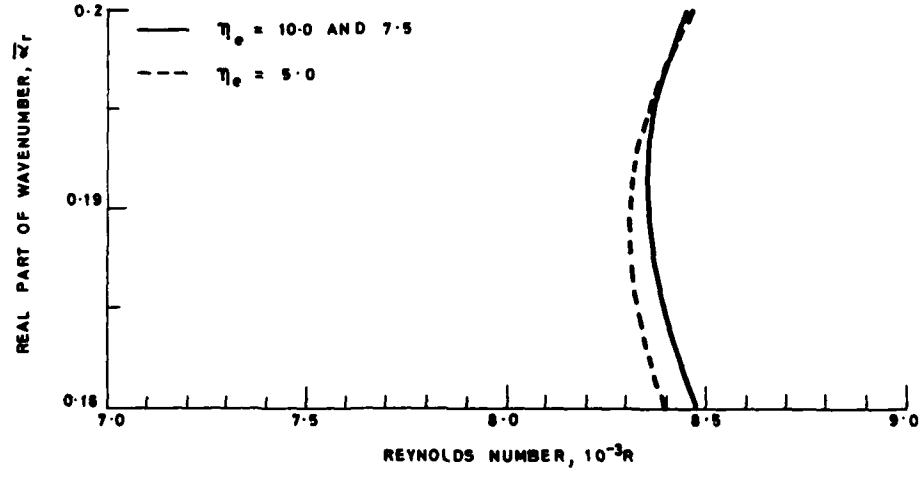

FIG. 6 EFFECT OF FREESTREAM BOUNDARY ON NEUTRAL STABILITY CURVE (HEATED PLATE, T_∞ = 15·6°C (60°F), T_w = 93·3°C (200°F))

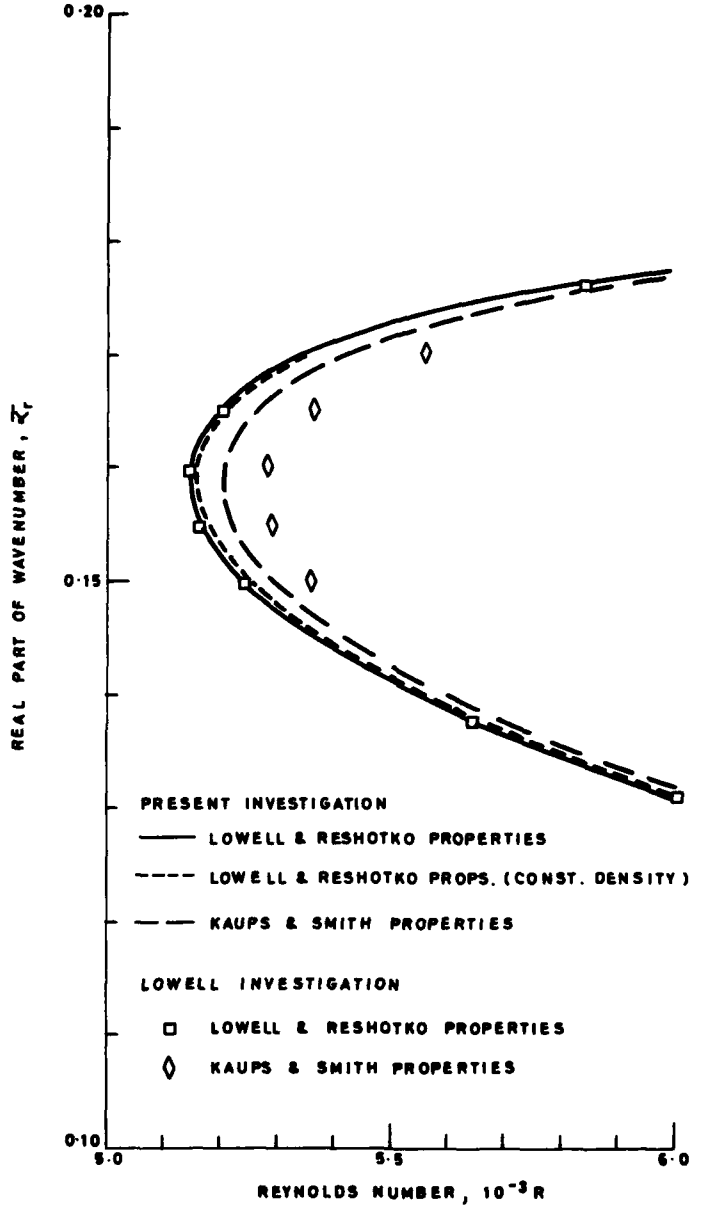

FIG. 7 EFFECT OF DIFFERENT FLUID PROPERTIES ON NEUTRAL STABILITY CURVE OF HEATED PLATE
(T_∞ = 15·6°C(60°F), T_W = 32·2°C (90°F))

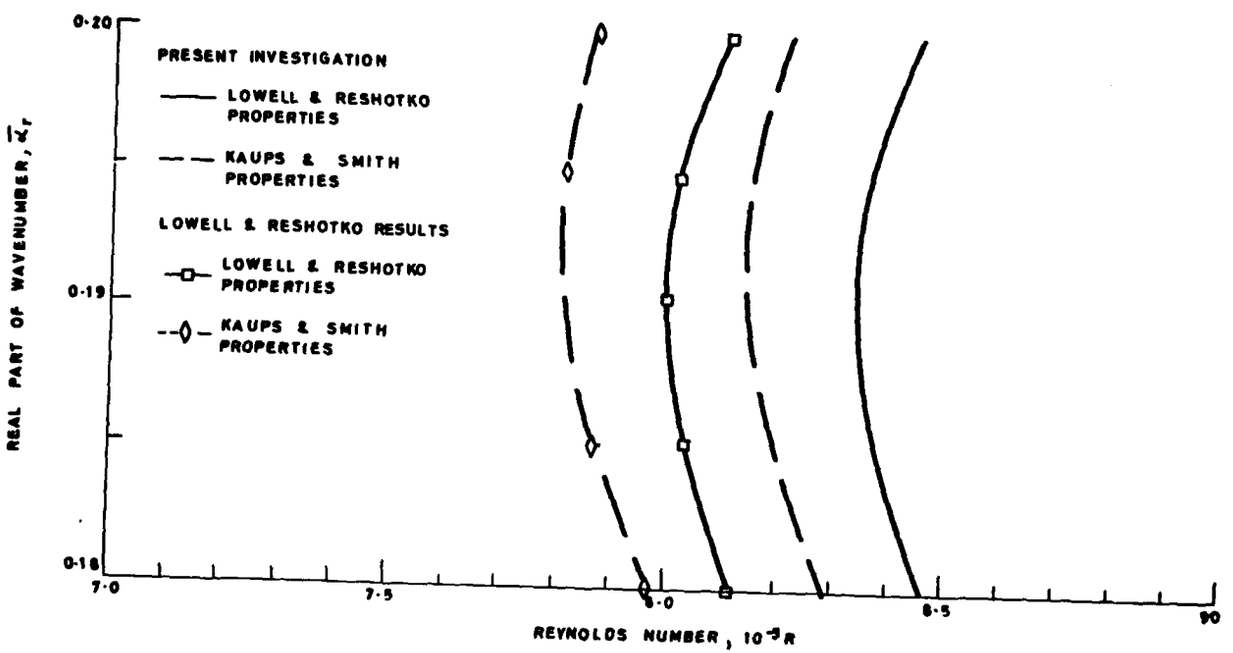

FIG. 8 EFFECT OF DIFFERENT FLUID PROPERTIES ON NEUTRAL STABILITY CURVE OF HEATED PLATE (T_{∞} = 15·6°C (60°F), T_W = 93·3° C (200° F))

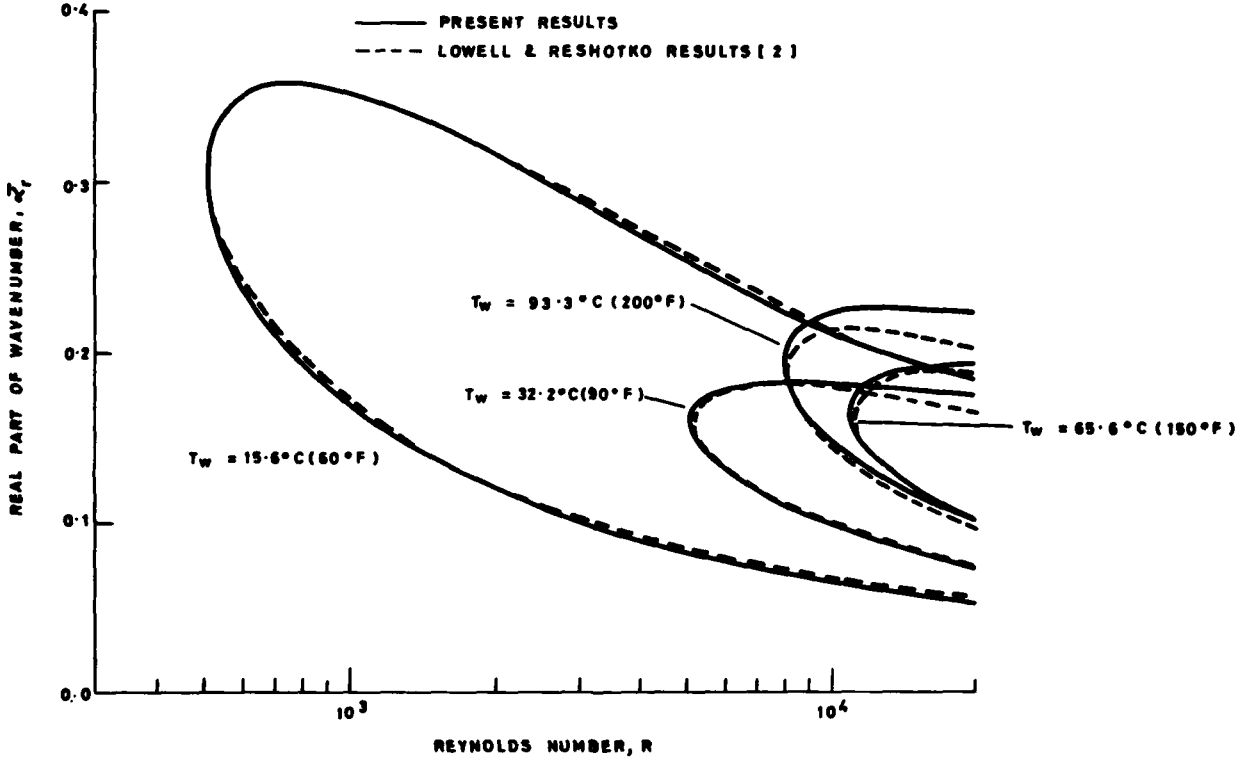

FIG. 9 EFFECT OF DIFFERENT WALL TEMPERATURES ON NEUTRAL STABILITY CURVE (T_∞ = 15·6°C (60°F))

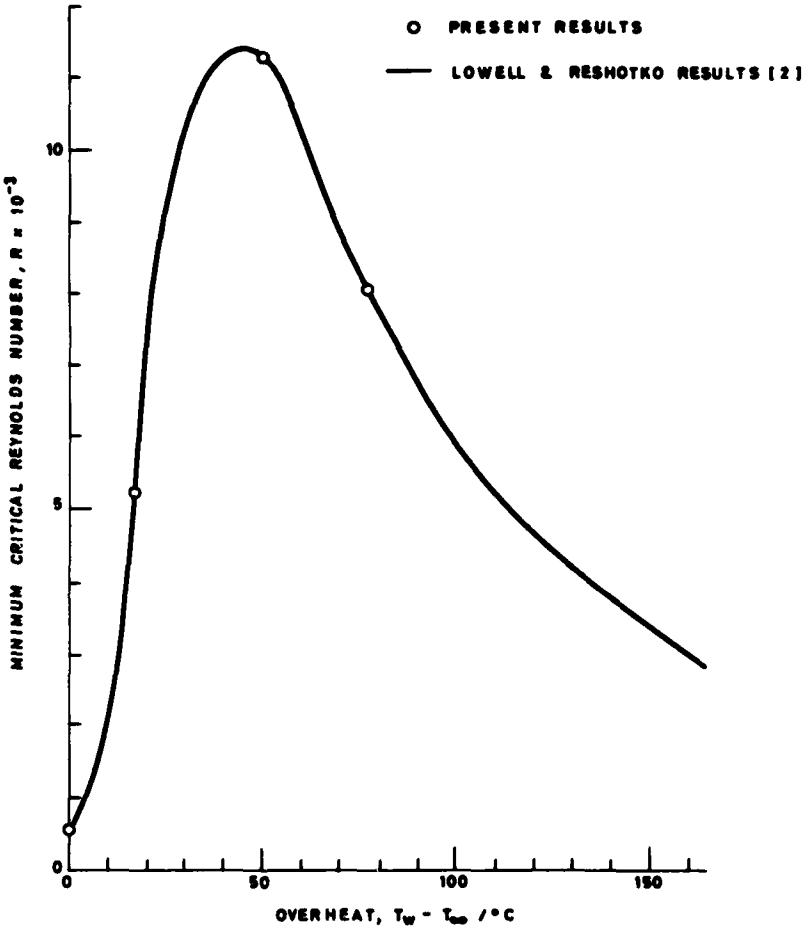

FIG. 10 EFFECT OF OVERHEAT ON MINIMUM CRITICAL REYNOLDS NUMBER

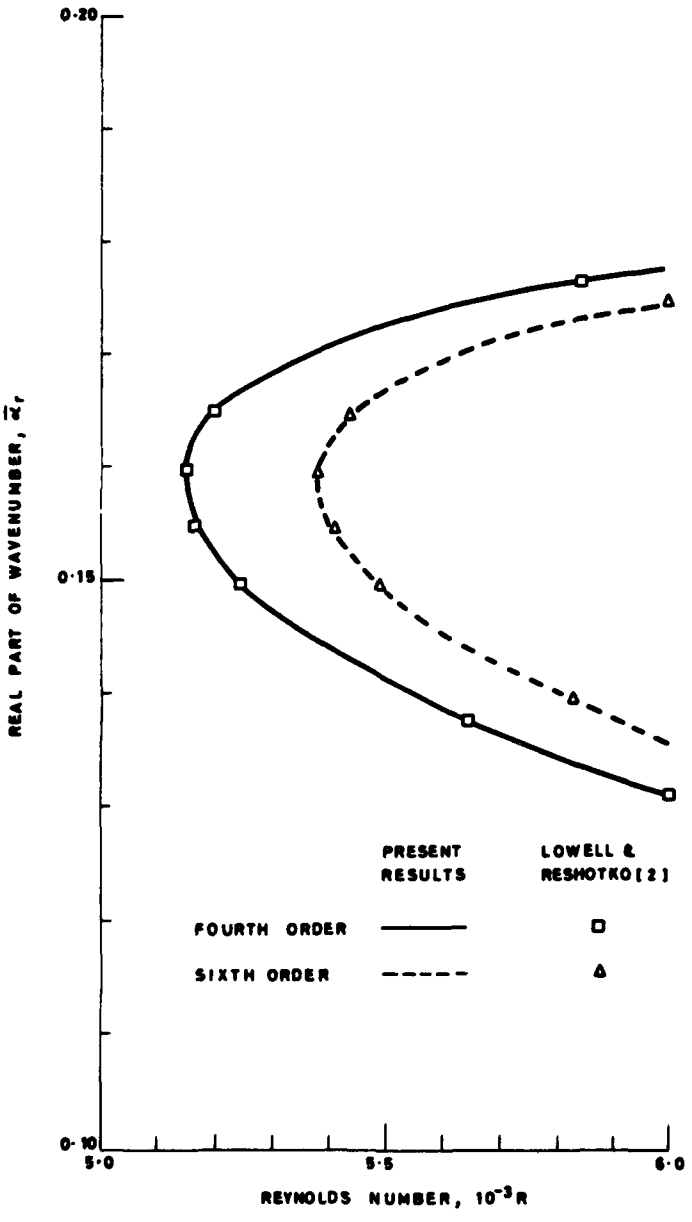

FIG. 11 COMPARISON OF NEUTRAL STABILITY CURVES USING FOURTH-AND SIXTH-ORDER APPROACHES

4. CONCLUSIONS AND SUGGESTIONS FOR FURTHER RESEARCH

The compound matrix method gives eigenvalues which generally agree with previously published results. Different expressions for the variation of fluid properties with temperature give nontrivial but small differences in calculated eigenvalues, as does the calculation of the mean flow using second- and fourth-order numerical methods. Calculations for heated flat plates with constant wall temperature suggest (in accordance with previous work) that the optimum overheat is about 40°C and that further heating has a destabilising effect on the boundary layer.

The sixth-order formulation, where fluctuations of all the flow variables are included, gives eigenvalues which are only slightly different from those obtained using the fourth-order formulation based on the modified Orr-Sommerfeld equation. It is not practicable to incorporate the method in a transition calculation procedure based on spatial instability, but further eigenvalue calculations, based on temporal instability, could be undertaken if thought desirable.

The compound matrix method requires a large number of integration steps (typically 800 to 1600) to obtain accurate eigenvalues. BMT Ltd [8] have proposed an alternative eigenvalue finder, based on a panel method, which requires relatively few integration steps. They demonstrated that the method works using a Blasius (unheated flat-plate) velocity profile in the temporal instability case. Further research would be necessary for a spatial stability implementation to be used in a transition prediction method and this might be useful if a large number of heated body calculations were required.

The compound matrix method is suitable for inclusion in a method for predicting boundary-layer transition on axisymmetric heated bodies. The fluid property relations for fresh water proposed by Lowell & Reshotko [2] are suitable for use in such a method. The assumption of constant density does not introduce any appreciable errors and it can be used to simplify an axi-symmetric calculation procedure and to reduce the computational effort. A second-order finite-difference boundary-layer calculation method could be used to determine the mean-flow profiles.

Although it simplifies the problem, the assumption of constant surface temperature is physically unrealistic. To maintain a constant surface temperature on a flat plate requires a non-uniform distribution of heat flux which makes the mean flow two-dimensional rather than one-dimensional. It is planned for future computations to prescribe either the surface temperature or the surface heat-flux which is allowed to vary with streamwise position.

5. ACKNOWLEDGMENTS

The author is grateful to Dr D L Randles of ARE(Portland) for supplying his computer programs for transition prediction on unheated bodies, and to Prof M Gaster, Dr P F Easthope and Messrs A P Daniel & G J K Willis of BMT Ltd for helpful discussions.

D J Atkins (SSO)

REFERENCES

1. SMITH,AMO & GAMBERONI,N. Transition, pressure gradient and stability theory. Douglas Aircraft Co. Rep. ES 26388 (1956)

2. LOWELL,RL. & RESHOTKO,E. Numerical study of a heated water boundary layer. Case Western Reserve University FTAS TR73-93 (1974)

3. KAUPS,K. & SMITH,AMO. The laminar boundary layer in water with variable properties. Proc ASME-AIChE Heat Transfer Conference, Seattle, Washington (ASME Paper 67-HT-69) (1967)

4. WILLIS,GJK. An eigenvalue finder for flows over a rigid heated surface. National Maritime Institute Report (1984). COMMERCIAL-IN-CONFIDENCE

5. DRAZIN,PG & REID,WH. Hydrodynamic stability. Cambridge University Press (1982)

6. EASTHOPE,PF. A sixth-order eigenvalue finder for the stability of flows over heated surfaces. British Maritime Technology Report (1986). COMMERCIAL-IN-CONFIDENCE

7. MILLER,GF & FERRISS,DH. Description of routines ORRSOM and INTEG. National Physical Laboratory Report (1980). COMMERCIAL-IN-CONFIDENCE

8. EASTHOPE,PF. A panel method for the numerical solution of the Orr-Sommerfeld equation. British Maritime Technology Report (1986). COMMERCIAL-IN-CONFIDENCE

9. SCHLICHTING,H. Boundary-layer theory. McGraw-Hill (7th Edn. 1978)

10. SMITH,AMO & CLUTTER,DW. Machine calculation of compressible boundary layers. AIAA J. 3(4)639-647 (1965)

11. KAY,GWC & LABY,TH. Tables of physical and chemical constants. Longman (14th Edn. 1973)

12. WEAST,RC et al. (Eds.) Handbook of Chemistry and Physics. The Chemical Rubber Co. (45th Edn. 1964)

13. NAG Library Manual, Mk 10 FORTRAN, Numerical Algorithms Group, Oxford (1983)

14. NACHTSHEIM,PR & SWIGERT,P. Satisfaction of asymptotic boundary conditions in numerical solution systems of nonlinear equations of boundary-layer type. NASA TN D-3004 (1965)

15. CEBICI,T. & SMITH,AMO. Analysis of turbulent boundary layers. Academic Press (1974)

16. CEBICI,T. & BRADSHAW,P. Momentum transfer in boundary layers. McGraw Hill (Hemisphere) (1977)

17. JORDINSON,R. The flat plate boundary layer. Part 1. Numerical integration of the Orr-Sommerfeld equation. J. Fluid Mech. 43(4)801-811 (1970)

18. GASTER,M. Series representation of the eigenvalues of the Orr-Sommerfeld equation. Paper 2 in AGARD-CP-224 (Laminar-turbulent transition) (1977)

Reports quoted are not necessarily available to members of the public or to commercial organizations.

APPENDIX A

Derivation of the mean flow equations for a heated body

This Appendix presents the equations of motion of a heated two-dimensional body and a heated flat plate. Let x represent the co-ordinate along the body surface and y the co-ordinate normal to the surface, with $u(x,y)$ and $v(x,y)$ the respective velocity components and $T(x,y)$ the absolute temperature. The fluid properties (density ρ, dynamic viscosity μ, specific heat C_p and thermal conductivity k) are assumed to be functions of temperature only. The usual boundary-layer assumptions are made, namely, that streamwise derivatives are much less than cross-stream ones. The equations of motion are [3]:-

Continuity:
$$\frac{\partial}{\partial x}(\rho u) + \frac{\partial}{\partial y}(\rho v) = 0 \qquad \text{(A1)}$$

Momentum:
$$\rho\left\{u \frac{\partial u}{\partial x} + v \frac{\partial v}{\partial y}\right\} = \rho_\infty u_e \frac{\partial u_e}{\partial x} + \frac{\partial}{\partial y}\left\{\mu \frac{\partial u}{\partial y}\right\} \qquad \text{(A2)}$$

Energy:
$$\rho C_p \left\{u \frac{\partial T}{\partial x} + v \frac{\partial T}{\partial y}\right\} = \frac{\partial}{\partial y}\left\{k \frac{\partial T}{\partial y}\right\} \qquad \text{(A3)}$$

In the momentum equation (A2), the buoyancy term,

$$g_x (\rho - \rho_\infty)$$

where g_x is the acceleration due to gravity in the freestream direction, has been neglected. This is equivalent to assuming that the flow is horizontal. In the energy equation (A3), the compression work term

$$-\frac{1}{\rho}\frac{d\rho}{dT} Tu \frac{\partial p}{\partial x}$$

has also been neglected, since $(-1/\rho)(d\rho/dT)$ (the coefficient of thermal expansion of water) is very small and the whole term is also small. The viscous dissipation term

$$\mu (\partial u/\partial y)^2$$

in the energy equation has been neglected, since Schlichting [10] has shown that it is negligible unless the Eckert number

$$E = u_\infty^2/(C_p T_\infty)$$

is of the order of unity. The value of E in the present application is of the order of 10^{-4}.

The velocity boundary conditions are:-

$$u = 0, \quad v = 0 \quad \text{on} \quad y = 0$$
$$u \to u_e \quad \text{as} \quad y \to \infty \tag{A4}$$

The temperature boundary condition at the wall is one of two options, that of prescribed wall temperature

$$T = T_w(x) \quad \text{on} \quad y = 0 \tag{A5}$$

or prescribed wall heat flux

$$-k\, \partial T/\partial y = \phi_w(x) \quad \text{on} \quad y = 0 \tag{A6}$$

The freestream temperature boundary condition is

$$T/T_\infty \to 1 \quad \text{as} \quad y \to \infty \tag{A7}$$

The above equations (A1) to (A3) with the boundary conditions (A4) to (A7) are transformed to a more convenient co-ordinate system by stretching the y co-ordinate. A modified Howarth-Dorotnitsyn transformation [10] is used, given by

$$\xi = x \tag{A8}$$

$$\eta = \left(\frac{\rho_\infty u_e}{\mu_\infty x}\right)^{1/2} \int_0^y \frac{\rho}{\rho_\infty}\, dy \tag{A9}$$

The stream function ψ is defined in the usual way, as

$$\rho u = \partial\psi/\partial y$$
$$\rho v = -\partial\psi/\partial x \tag{A10}$$

and a dimensionless stream function $f(\eta)$ is defined by

$$\partial f/\partial \eta = u/u_e \tag{A11}$$

f is related to ψ as follows:

$$\psi = (\rho_\infty \mu_\infty u_e \xi)^{1/2} f \tag{A12}$$

The dimensionless temperature $g(\eta)$ is defined by

$$g = T/T_\infty \tag{A13}$$

The equations of motion are transformed to ξ, η co-ordinates using the following relations:

$$\frac{\partial}{\partial x} = \frac{\partial}{\partial \xi} - \frac{1}{2}\frac{\eta}{\xi}\frac{\partial}{\partial \eta} + \eta\,(I_1/I_2)\,\frac{\partial}{\partial \eta} \tag{A14}$$

where $$I_1 = \int_0^y (\partial\rho/\partial x)\ dy$$

and $$I_2 = \int_0^y \rho\psi\ dy$$

$$\frac{\partial}{\partial y} = \left\{\frac{u_e}{\rho_\infty \mu_\infty \xi}\right\}^{1/2} \rho\,\frac{\partial}{\partial \eta} \tag{A15}$$

The continuity equation is automatically satisfied by the definition of the stream function. After transformation, the momentum and energy equations become

$$\frac{\partial}{\partial \eta}(C\,f'') + \frac{m+1}{2}\,f\,f'' + m\left\{\frac{\rho_\infty}{\rho} - f'^2\right\} = \xi\left\{f'\,\frac{\partial f'}{\partial \xi} - f''\,\frac{\partial f}{\partial \xi}\right\} \tag{A16}$$

$$\left\{Pr_\infty\,\bar{C}_p\right\}\ \frac{\partial}{\partial \eta}(K\,g') + \frac{m+1}{2}\,f\,g' = \xi\left\{f'\,\frac{\partial g}{\partial \xi} - g'\,\frac{\partial f}{\partial \xi}\right\} \tag{A17}$$

In equations (A16) and (A17), dashes denote differentiation with respect to η, and

$$C = \frac{\rho\,\mu}{\rho_\infty\,\mu_\infty}, \qquad K = \frac{\rho\,k}{\rho_\infty\,k_\infty}$$

$$m = \frac{\xi}{u_e}\frac{du_e}{d\xi}$$

$$Pr_\infty = \frac{\mu_\infty\,C_{p\infty}}{k_\infty}, \qquad \bar{C}_p = \frac{C_p}{C_{p\infty}}$$

m is a dimensionless pressure gradient parameter and Pr_∞ a freestream Prandtl number. The transformed boundary conditions are:

$$f(0) = 0, \qquad f'(0) = 0 \tag{A18}$$

and either

$$g(0) = g_w \tag{A19}$$

or

$$g'(0) = g'_w \tag{A20}$$

As $\eta \to \infty$,

$$f'(\eta) \to 1, \qquad g(\eta) \to 1 \tag{A21}$$

Equations (A16) and (A17) along with the boundary conditions (A18) to (A21) describe the mean flow over a heated two-dimensional body. In the case of a flat plate, assuming similarity of the velocity and temperature profiles, m is zero and (A16) and (A17) simplify to

$$\frac{\partial}{\partial \eta} (C f'') + \frac{1}{2} f f'' = 0 \tag{A22}$$

$$\left(Pr_\infty \bar{C}_p\right)^{-1} \frac{\partial}{\partial \eta} (K g') + \frac{1}{2} f g' = 0 \tag{A23}$$

For an unheated plate, equation (A22) reduces to the well-known Blasius equation

$$f''' + \frac{1}{2} f f'' = 0 \tag{A24}$$

A P P E N D I X B

Fluid-property relations

The mean flow calculation procedure requires values for density, viscosity and thermal conductivity and their first derivatives and values for specific heat capacity, all expressed as functions of temperature. The numerical procedure used by Lowell & Reshotko [2] requires, in addition, one further derivative of each quantity.

Two sets of fluid property relations were used in the present investigations. Those proposed and used by Lowell & Reshotko [2] are as follows:

Specific heat capacity

$$C_p/C_{p0} = 2{\cdot}13974 - 9{\cdot}68137\times10^{-3}\,T + 2{\cdot}68536\times10^{-5}\,T^2 - 2{\cdot}42139\times10^{-8}\,T^3 \quad (T \text{ in K}) \qquad (B1)$$

Density

$$\frac{\rho}{\rho_0} = 1 - \frac{(T-a)^2\,(T+b)}{c(T+d)} + e\,\exp(-f/T) \qquad (B2)$$

$$\frac{1}{\rho_0}\frac{d\rho}{dt} = \frac{1}{(T+d)}\left[-\frac{(T-a)(3T-2b-a)}{c} + 1 - \frac{\rho}{\rho_0} + \frac{e}{T^2}\exp(-f/T)\,\{T^2 + f(T+d)\}\right] \qquad (B3)$$

$$\frac{1}{\rho_0}\frac{d^2\rho}{dT^2} = -\frac{2}{\rho_0}\frac{d\rho}{dT} + \frac{1}{(T+d)}\left[\frac{(-6T+4a-2b)}{c} + \frac{ef}{T^4}\{(f-2d)T+fd\}\exp(-f/T)\right] \qquad (B4)$$

In equations (B2) to (B4), T is in °C and

a = 3·9863, b = 288·9414, c = 508929·2, d = 68·12963,

e = 0·011445 and f = 374·3

Dynamic viscosity

$$\log_{10}(a\,\mu_0/\mu) = \frac{b(T-20) + c(T-20)^2}{d+T} \qquad \text{(B5)}$$

$$\frac{1}{\mu_0}\frac{d\mu}{dt} = -(\mu_0/\mu)\left\{\frac{b + 2c(T-20) - \log_{10}(a\,\mu_0/\mu)}{e(d+T)}\right\} \qquad \text{(B6)}$$

$$\frac{1}{\mu_0}\frac{d^2\mu}{dT^2} = -2\left\{\frac{\mu\, c}{\mu_0 e} + \frac{1}{\mu_0}\frac{d\mu}{dT}\right\} + \frac{1}{\mu\,\mu_0}\left\{\frac{d\mu}{dT}\right\}^2 \qquad \text{(B7)}$$

In equations (B5) to (B7), T is in °C and

$a = 1{\cdot}002$, $b = 1{\cdot}37023$, $c = 8{\cdot}36\times10^{-4}$, $d = 109{\cdot}0$, $e = 0{\cdot}43429448$

Thermal conductivity

$$k/k_0 = -9{\cdot}90109 + 0{\cdot}1001982\,T - 1{\cdot}873892\times10^{-4}\,T^2 + 1{\cdot}039570\times10^{-7}\,T^3 \qquad \text{(B8)}$$

Expressions for the derivatives of C_p/C_{p0} and k/k_0 can easily be obtained from equations (B1) and (B8). In the above expressions,

$$C_{p0} = 4186{\cdot}8\ \text{J kg}^{-1}\text{K}^{-1}\ ,\quad \rho_0 = 1000\ \text{kg m}^{-3},$$
$$\mu_0 = 0{\cdot}001\ \text{N s m}^{-2},\quad k_0 = 0{\cdot}1\ \text{W m}^{-1}\text{K}^{-1} \qquad \text{(B9)}$$

The value of C_{p0} differs slightly from that used by Lowell & Reshotko, but this has been shown to have a negligible effect on the numerical results.

A different set of expressions were proposed by Kaups & Smith [3], who fitted least-square polynomials to the normalised experimental data to give

$$\frac{C_p}{C_{p,ref}} = 1{\cdot}4833689 - 0{\cdot}8072501\,\frac{T}{T_{ref}} + 0{\cdot}3289602\left\{\frac{T}{T_{ref}}\right\}^2 \qquad (B10)$$

$$\frac{\rho}{\rho_{ref}} = 0{\cdot}803928 + 0{\cdot}4615901\,\frac{T}{T_{ref}} - 0{\cdot}2869774\left\{\frac{T}{T_{ref}}\right\}^2 + 0{\cdot}0234689\left\{\frac{T}{T_{ref}}\right\}^3 \qquad (B11)$$

$$\frac{\mu}{\mu_{ref}} = \left[a + b\,\frac{T}{T_{ref}} + c\left\{\frac{T}{T_{ref}}\right\}^2 + d\left\{\frac{T}{T_{ref}}\right\}^3 + e\left\{\frac{T}{T_{ref}}\right\}^4\right]^{-1} \qquad (B12)$$

where $a = 35{\cdot}15539$, $b = -106{\cdot}9718715$, $c = 107{\cdot}7720376$, $d = -40{\cdot}5953074$, and $e = 5.6391948$.

$$\frac{T_{ref}}{\mu_{ref}}\,\frac{d\mu}{dT} = -\left\{\frac{\mu}{\mu_{ref}}\right\}\left[b + 2c\left\{\frac{T}{T_{ref}}\right\} + 3d\left\{\frac{T}{T_{ref}}\right\}^2 + 4e\left\{\frac{T}{T_{ref}}\right\}^3\right] \qquad (B13)$$

$$\frac{k}{k_{ref}} = -1{\cdot}940589 + 5{\cdot}2220185\left\{\frac{T}{T_{ref}}\right\} - 2{\cdot}693322\left\{\frac{T}{T_{ref}}\right\}^2 + 0{\cdot}4176176\left\{\frac{T}{T_{ref}}\right\}^3 \qquad (B14)$$

The reference values in the above expressions are:

$T_{ref} = 273{\cdot}15$ K, $C_{p,ref} = 4218$ J kg^{-1}K^{-1}, $\rho_{ref} = 999{\cdot}84$ kg m^{-3}, $\mu_{ref} = 0{\cdot}0017936$ N s m^{-2} and $k_{ref} = 0{\cdot}5537$ W m^{-1}K^{-1} (B15)

Figures 12 (a) to (d) show comparisons of the two sets of formulae for C_p, ρ, μ and k compared with known values [11,12] in the range 0-100°C (273·15-373·15 K). There is little difference between them for μ and k, but Lowell's expressions agree more favourably with the known values for C_p and ρ. The Kaups & Smith formulae were designed to fit the data over a much wider temperature range than that of interest in the present investigation. The formulae of Lowell & Reshotko are recommended for use in future investigations.

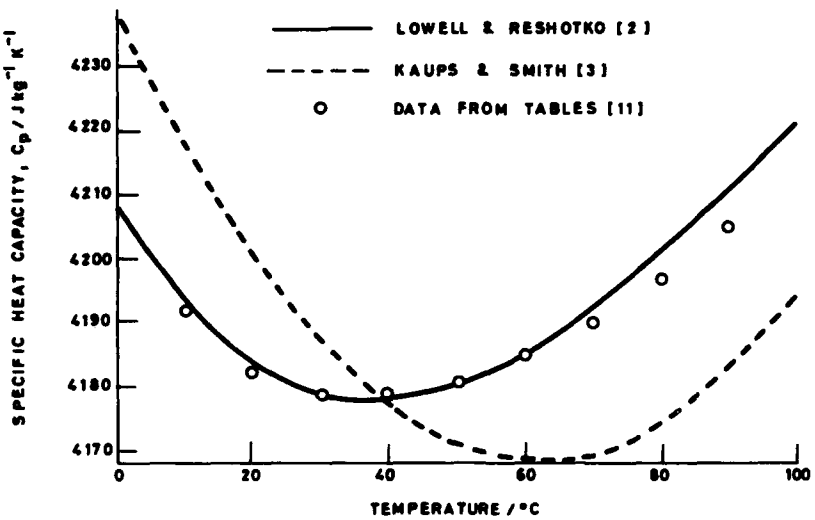

FIG. 12(a) COMPARISON OF DIFFERENT FORMULAE FOR SPECIFIC HEAT CAPACITY WITH DATA FROM TABLES

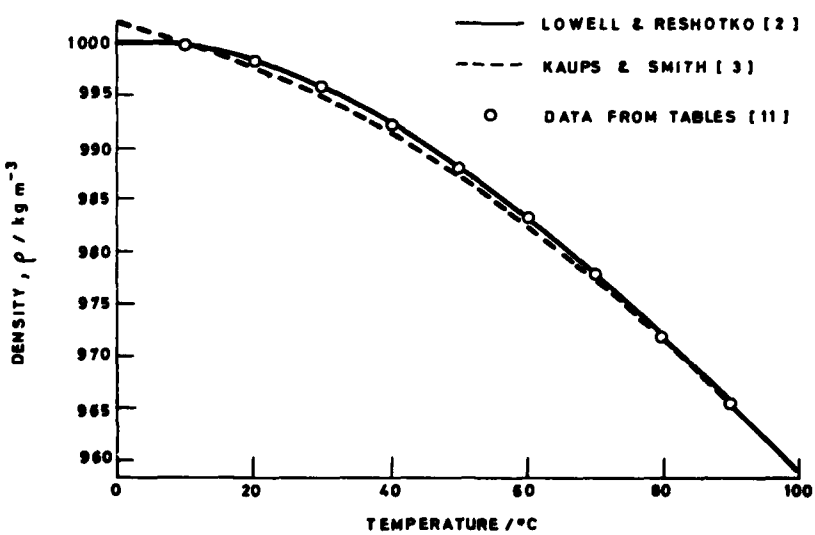

FIG. 12(b) COMPARISON OF DIFFERENT FORMULAE FOR DENSITY WITH DATA FROM TABLES

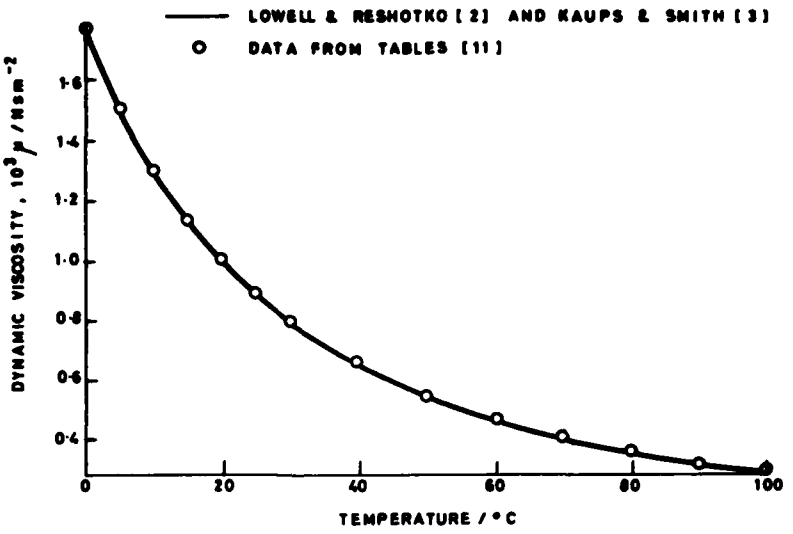

FIG. 12 (c) COMPARISON OF DIFFERENT FORMULAE FOR DYNAMIC VISCOSITY WITH DATA FROM TABLES

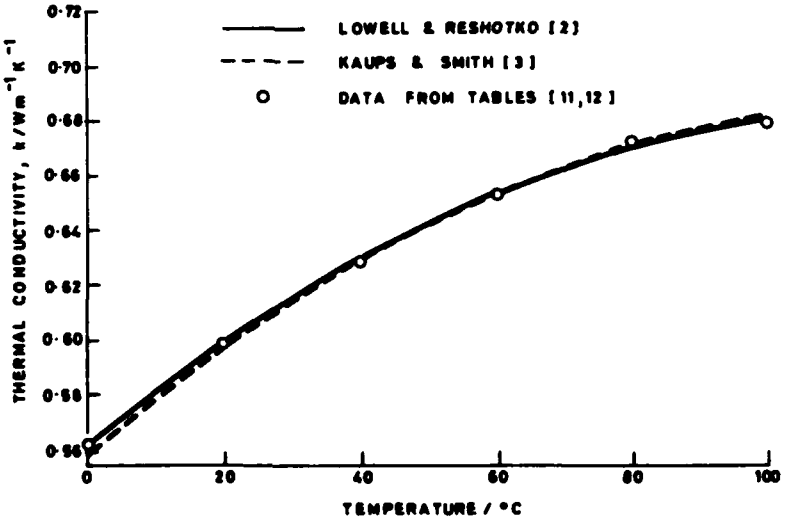

FIG. 12(d) COMPARISON OF DIFFERENT FORMULAE FOR THERMAL CONDUCTIVITY WITH DATA FROM TABLES

A P P E N D I X C

Computation of the mean flow profiles

The mean flow problem, defined by equations (A22) and (A23) with boundary conditions (A18), (A19) and (A21) is a two-point non-linear boundary-value problem. Two NAG Library [13] routines exist for this type of problem, one called D02GAF (Method 1), based on a finite-difference type method, and the other called D02HAF (Method 2), based on a shooting and matching method. To use these methods, equations (A22) and (A23) have to be recast in a slightly different form, viz:

$$f''' = -\left(\frac{1}{\rho}\frac{\partial\rho}{\partial T} + \frac{1}{\mu}\frac{\partial\mu}{\partial T}\right) T_\infty\, g'\, f'' - \frac{\rho_\infty\,\mu_\infty}{2\,\rho\,\mu}\, f\, f'' \qquad (C1)$$

$$g'' = -\left(\frac{1}{\rho}\frac{\partial\rho}{\partial T} + \frac{1}{k}\frac{\partial k}{\partial T}\right) T_\infty\, g'^2 - C_p\, Pr_\infty \frac{\rho_\infty\, k_\infty}{2\,\rho\, k}\, f\, g' \qquad (C2)$$

Rather than calculating out to infinity, the freestream boundary conditions are applied at some value η_e which is specified as a numerical parameter. Most of the present calculations were carried out using $\eta_e = 10$. In practice, a smaller value may be acceptable for engineering calculations. Initial estimates have to be supplied for all the boundary values, i.e. f, f', f'', g and g' at $\eta = 0$ and $\eta = \eta_e$. The boundary values supplied were:

$f''(0) = 1.0$ for unheated boundary layers,

$f''(0) = 0.5$ for heated boundary layers,

$g'(0) = -0.05$

$f(\eta_e) = \eta_e - 2$

$f''(\eta_e) = 0.0$

$g'(\eta_e) = 0.0$

For a time, the author did not have access to the NAG Library, and so a third method was tried. This method is the one used by Lowell & Reshotko [2] and is based on a special technique used for handling asymptotic boundary conditions described by Nachtstein & Swigert [14]. Both references give FORTRAN listings. This method only requires initial estimates for $f''(0)$ and $g'(0)$ annd the values used for these were the same as those used in Methods 1 and 2.

All three methods were used to obtain mean flow profiles for the unheated case and for the heated cases examined by Lowell. The main numerical parameters are presented in Table 1. It proved difficult to obtain solutions using Method 1, with η_e

having a value of 10 in all the heated cases, but some solutions were obtained with smaller values of η_e giving slightly different answers. The values of $f''(0)$ and $g'(0)$ using Methods 2 and 3 agree with each other to eight decimal places and they agree with the values of Lowell to at least four decimal places. Method 2 was found easiest to use as the output profiles could be expressed on an arbitrary grid of points, and this was the method used for most of the computations.

The same profiles were computed using a second-order finite-difference method which is well documented in the literature [15,16] and referred to as Method 4 here. The wall-shear parameters were slightly different from those using fourth-order methods where these have converged. The effect of these differences is shown in Appendices D and E.

Calculations using the NAG library routines were carried out in double precision arithmetic (64-bit word length). Most of the other calculations were in single precision arithmetic (32-bit word length). In general, double precision made no appreciable difference compared with single precision.

Temperature (°C)			Freestream	Wall shear	Wall heat flux
Ambient	Wall	Method	Boundary	$f''(0)$	$g'(0)$
15.5556	15.5556	1	10	0.33205734	
		2	10	0.33205734	
		3	10	0.33205734	
		Lowell	10	0.33205733	
		4	10	0.33203962	
15.5556	32.2222	1	10	0.46640722	-0.04118285
		2	10	0.46640722	-0.04118285
		3	10	0.46640722	-0.04118285
		Lowell	10	0.46639971	-0.04117200
		4	10	0.46631959	-0.04124339
15.5556	65.5556	1	5	0.74604546	-0.13595093
		2	10	0.74322894	-0.13577964
		3	10	0.74322893	-0.13577963
		Lowell	10	0.74319378	-0.13574200
		4	10	0.74280715	-0.13596509
15.5556	93.3333	1	8	0.96324417	-0.22613273
		2	10	0.96324381	-0.22613270
		3	10	0.96324381	-0.22613270
		Lowell	10	0.96317694	-0.22606900
		4	10	0.96232432	-0.22641809

Table I Comparison of mean-flow wall parameters using different numerical methods

The effect of different fluid property relations on the mean flow parameters and the displacement thickness δ^* is shown in Table II. All computations were using Method 2 with an ambient temperature of 15.5556°C and the freestream boundary at $\eta = 10$. The results show that different property relations give small differences in the numerical parameters, but the assumption of constant density has hardly any effect.

Wall Temp (°C)	Fluid Properties	Wall shear $f''(0)$	Wall heat flux $g'(0)$	Displacement thickness δ^*
15.5556		0.332057		1.720788
32.2222	Lowell	0.466407	-0.041183	1.514571
	Lowell (const ρ)	0.466429	-0.041212	1.514638
	Kaups & Smith	0.467292	-0.041341	1.514442
65.5556	Lowell	0.743329	-0.135780	1.211281
	Lowell (const ρ)	0.743271	-0.135667	1.211291
	Kaups & Smith	0.743302	-0.135909	1.211802
93.3333	Lowell	0.963244	-0.226133	1.037017
	Lowell (const ρ)	0.963143	-0.225632	1.036866
	Kaups & Smith	0.959619	-0.225790	1.038404

Table II Comparison of mean-flow wall parameters using different fluid property relations

APPENDIX D

Detailed numerical results for unheated plates

Numerical results for the stability of the Blasius boundary layer corresponding to an unheated plate have been published in the literature by Jordinson [17] for the case of spatial instability and by Davey (referenced by Gaster [18]) for the case of temporal instability. For comparison with these results, eigenvalues were calculated using 800 integration steps in the former case and 3200 steps in the latter case, with the free-stream boundary at $\eta = 10$. Table III shows comparisons for the spatial instability case and Table IV for the temporal instability case.

		Present investigation		Jordinson [17]	
Reynolds Number	Frequency $\bar{\omega}$	Wave number $\bar{\alpha}$ Real	Imag	Wave number $\bar{\alpha}$ Real	Imag
336	0.1297	0.308349	0.007940	0.3084	0.0079
598	0.1201	0.307848	-0.001897	0.3079	-0.0019
998	0.1122	0.308596	-0.005710	0.3086	-0.0057

Table III Comparison of eigenvalues with those of Jordinson [17]

		Present investigation		Davey [18]	
Reynolds Number	Frequency $\bar{\omega}$	Wave number $\bar{\alpha}$ Real	Imag	Wave number $\bar{\alpha}$ Real	Imag
500	0.3	0.11930379	-0.00027998	0.11930376	-0.00027998
1500	0.2	0.06312283	0.00315660	0.06312291	0.00315663
3000	0.15	0.04021918	0.00278070	0.04021919	0.00278079

Table IV Comparison of eigenvalues with those of Davey [18]

Engineering calculations of transition on axisymmetric bodies are normally carried out using a second-order accurate finite-difference method [15,16] as opposed to the fourth-order-accurate methods used specifically for a flat plate calculation. To see whether this made any significant difference to the eigenvalues, some further tests were carried out using the Blasius boundary layer calculated in three different ways. These were (a) a fourth-order calculation using Method I (see Appendix C), (b) a second-order finite difference calculation using a modified version of the program described in Reference 15, with the second derivative of velocity $f'''(\eta)$ calculated using a second-order finite-difference approximation, and (c) with the velocity $f'(\eta)$ calculated using a second-order method and $f'''(\eta)$ calculated exactly from the differential equation (A24). The results using all three methods are tabulated, along with Jordinson's results in Table V. In all cases, the freestream boundary was at $\eta = 10$ and 800 integration steps were used.

Reynolds Number	Frequency $\bar{\omega}$	Method	Wave number $\bar{\alpha}$ Real	Imag
336	0.1297	(a)	0.30835	0.00793
		(b)	0.30828	0.00798
		(c)	0.30842	0.00794
		Jordinson	0.3084	0.0079
598	0.1201	(a)	0.30785	-0.00190
		(b)	0.30779	-0.00184
		(c)	0.30792	-0.00190
		Jordinson	0.3079	-0.0019
998	0.1122	(a)	0.30860	-0.00571
		(b)	0.30856	-0.00565
		(c)	0.30866	-0.00572
		Jordinson	0.3086	-0.0057

Table V Comparison of eigenvalues using different mean flows

Reynolds Number	Freq $\bar{\omega}$	No of Steps	Compound matrices Wave Number $\bar{\alpha}$ Real	Imag	NPL Method Wave number $\bar{\alpha}$ Real	Imag
400	0.02	3200	0.068109	0.026870	Failed to converge	
		1600	0.068109	0.026870	0.073973	0.028631
		800	0.068109	0.026871	0.069476	0.027321
		400	0.068111	0.026872	0.068446	0.026987
		200	0.068122	0.026895	0.068200	0.026915
		100	0.068357	0.027173	0.068162	0.026943
400	0.15	3200	0.355209	0.005268	0.363537	0.003345
		1600	0.355209	0.005268	0.357208	0.004773
		800	0.355209	0.005268	0.355703	0.005160
		400	0.355222	0.005265	0.355331	0.005306
		200	0.355379	0.005206	0.355235	0.005538
		100	0.356780	0.004176	0.355187	0.006365
1000	0.01	3200	0.279828	-0.007287	0.290591	-0.009000
		1600	0.279828	-0.007287	0.282377	-0.007763
		800	0.279832	-0.007289	0.280454	-0.007387
		400	0.279884	-0.007313	0.279976	-0.007224
		200	0.280443	-0.007734	0.279832	-0.006920
		100	0.282826	-0.013448	0.279681	-0.005818
2200	0.15	3200	0.390733	0.039061	0.402942	0.035210
		1600	0.390736	0.039060	0.393718	0.038130
		800	0.390776	0.039051	0.391486	0.038786
		400	0.391265	0.038833	0.390966	0.038816
		200	0.394557	0.034749	0.390944	0.038324
		100	0.382908	0.011654	0.391034	0.036591
10000	0.03	3200	0.135634	-0.011900	0.156262	-0.011298
		1600	0.135645	-0.011905	0.140224	-0.012065
		800	0.135774	-0.011985	0.136744	-0.011925
		400	0.136942	-0.013373	0.135896	-0.011769
		200	0.134532	-0.027835	0.135639	-0.011321
		100	0.101152	-0.032060	0.135369	-0.009668
10000	0.15	3200	0.389878	0.036309	0.400500	0.032976
		1600	0.389923	0.036298	0.392460	0.035479
		800	0.390448	0.036039	0.390498	0.036111
		400	0.393632	0.031597	0.389957	0.036295
		200	0.379159	0.010141	0.389628	0.036469
		100	0.310466	0.036128	0.388832	0.037578

Table VI Effect of number of integration steps on eigenvalues

Some comparisons were made of the number of integration steps on the eigenvalues. The comparisons were made using both the compound matrix method and a much older finite-difference type matrix method developed at NPL [17], which was supplied by ARE (Portland). Eigenvalues were generated starting with a Blasius profile at 101 points and converting the data to the required number of integration steps using the modified version of program NMIAL514. The freestream boundary was at $\eta = 10$. The results are presented in Table VI above. They show that the compound matrix method produces eigenvalues which converge to a "true" value as the number of integration steps is increased. At high Reynolds numbers, 800 steps are required to produce reasonably accurate eigenvalues. The NPL method, when used with 100 to 800 steps, gives eigenvalues which do not change very much with the number of steps. The eigenvalues generally lie within 1% of the "true" value, except near the region of neutral stability where $\bar{\alpha}_i$ is small. Above 800 steps, however, the method appears to suffer from ill-conditioning. It is implemented in double precision (64-bit word length).

Some numerical problems were encountered when using the compound matrix method. At high Reynolds numbers and high wave numbers, premature convergence occured, owing to a floating-point underflow condition. The problem could be cured by running in double precision with a special option known as G_FLOATING, where the smallest positive floating-point number is approximately 10^{-308}, as opposed to single precision and conventional double precision where the corresponding number is approximately 10^{-38}. However, this required twelve times the cpu time compared with the single precision version. The errors arising from this problem were generally in the sixth place of decimals, and only occurred in cases when $\bar{\alpha}_i$ was relatively large and positive, hence being of no real significance in a practical transition calculation.

In some cases, the eigenvalue calculation was sensitive to the initial guess. This problem occurred when using single precision and double precision arithmetic, both with and without the G_FLOATING option. Some numerical experiments were conducted using a Blasius profile calculated at 81 points with the freestream boundary at $\eta = 8$ and interpolated to 801 points (800 integration steps). Both modes 1 and 2 (spatial instability modes) were tried with a range of initial guesses for $\bar{\alpha}_r$ and $\bar{\alpha}_i$ (mode 1) and $\bar{\alpha}_i$ and $\bar{\omega}_r$ (mode 2). The results are shown in Figures 13 (mode 1) and 14 (mode 2). They show that at high Reynolds numbers, the convergence of the compound matrix method is sensitive to the initial guess. In particular, when using mode 1, to have any chance of convergence, the initial guess for $\bar{\alpha}_r$ should err on the low side, and with mode 2, the initial guess for $\bar{\omega}_r$ should err on the high side. Over the range of Reynolds

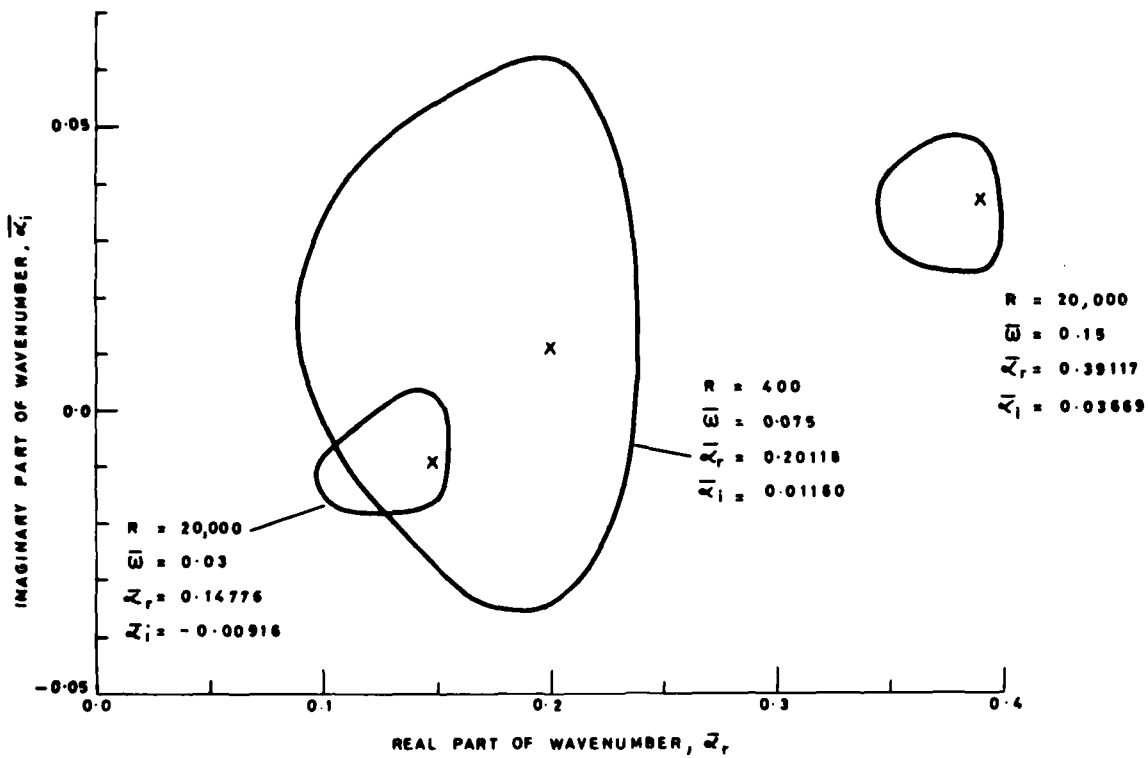

FIG. 13 GRAPH SHOWING AREA OF CONVERGENCE FOR TYPICAL EIGENVALUE CALCULATIONS USING MODE 1

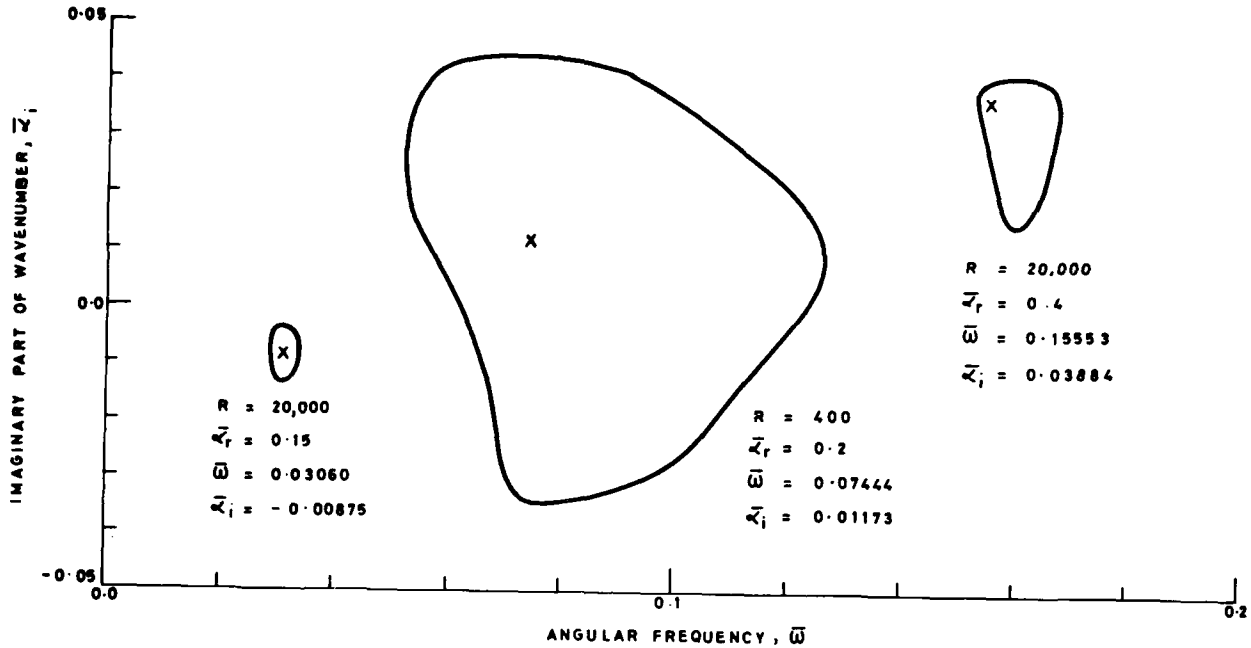

FIG.14 GRAPH SHOWING AREA OF CONVERGENCE FOR TYPICAL EIGENVALUE CALCULATIONS USING MODE 2

numbers tested (400 to 20000) this was only found to be a problem with unheated boundary layers at Reynolds numbers above 1000.

Although the eigenvalue calculation method was initially supplied as an interactive program, many of the computations involved generating a series of eigenvalues over a range of Reynolds number and wave number. Initially, the results of one eigenvalue calculation were used as the initial guess for another, but this method often failed at high Reynolds numbers. To overcome this difficulty, the following procedure was adopted. In mode 2, used for most of the calculations, for the lowest Reynolds number and the smallest value of $\bar{\alpha}_r$, user-specified values of $\bar{\alpha}_i$ and $\bar{\omega}_r$ were used as initial guesses. The resulting value of $\bar{\alpha}_i$ was used as the initial guess at the next value of $\bar{\alpha}_r$ and the initial guess for $\bar{\omega}_r$ was based on linear extrapolation with $\bar{\alpha}_r$. At the second lowest Reynolds number, for each $\bar{\alpha}_r$, the corresponding values of $\bar{\alpha}_i$ and $\bar{\omega}_r$ at the first Reynolds number were used as initial guesses. At higher Reynolds numbers, for a particular $\bar{\alpha}_r$, the initial guesses for $\bar{\alpha}_i$ and $\bar{\omega}_r$ were calculated using linear extrapolation with ln(R). This procedure worked well for all the heated cases, but no scheme could be found which worked successfully for all the unheated cases tested.

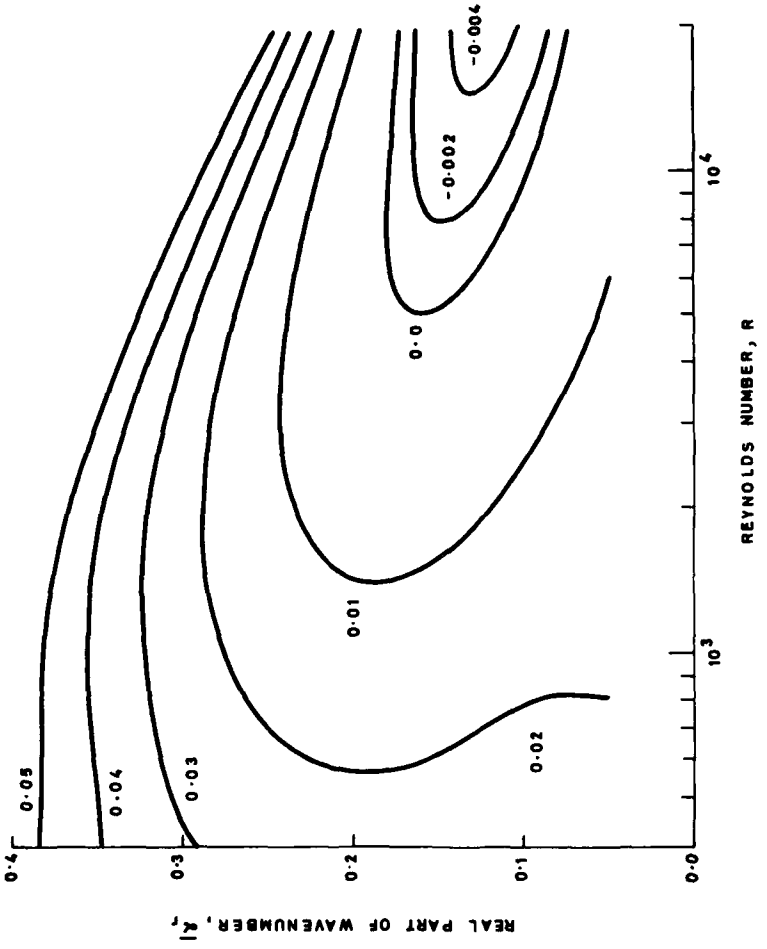

FIG. 15 TYPICAL PLOT OF CONTOURS OF $\bar{\alpha}_i$ AS A FUNCTION OF $\bar{\alpha}_r$ AND REYNOLDS NUMBER FOR A HEATED PLATE

A P P E N D I X E

Detailed numerical results for heated plates

The effect of using different numbers of integration steps on a few typical eigenvalue calculations using mode 2 is shown in Table VII below. The results show that a large number of integration steps are required to predict the eigenvalues accurately. In particular, to obtain accurate values in unstable regions, where the imaginary part of the wave number is negative, at least 1600 steps are required.

The effect of different mean velocity and temperature profiles on eigenvalue calculation is shown in Table VIII below. Different profiles were obtained by using different expressions for the fluid property variation with temperature. Three sets of expressions were used, being those of Lowell & Reshotko [2] with both variable and constant density, and those of Kaups & Smith [3]. These profiles were obtained for each value of wall temperature, using a fourth-order "exact" solution (Method 2 in Appendix C). A fourth set of profiles was obtained using a second-order "approximate" finite-difference solution (Method 4 in Appendix C), with the Lowell & Reshotko expressions for fluid-property variation with variable density. The results in Table VIII indicate that for a particular wall temperature, small changes in the mean-flow profiles (which are quantified in Appendix C) lead to relatively small changes in the eigenvalues. In particular, the assumption of constant density hardly affects the eigenvalue calculation. An errors obtained using this assumption are likely to be smaller than errors obtained using too few integration steps.

A typical plot of contours of $\bar{\alpha}_i$ as a function of R and $\bar{\alpha}_r$ is presented as Figure 15. In this case, the wall temperature is 32.2°C (90°F) and the Lowell & Reshotko property variation is used with 800 integration steps. The results using 1600 steps show only very slight differences in the unstable region ($\bar{\alpha}_r$ negative).

Figure 15 was obtained by computing a table of eigenvalues for a few values of $\bar{\alpha}_r$ and R (normally eight and ten respectively) using mode 2. To produce a smooth contour plot and to save on computer time, a much larger table of eigenvalues was generated for 51 uniformly-spaced values of $\bar{\alpha}_r$ and 51 uniformly-spaced (on a logarithmic scale) values of R, using cubic spline interpolation (NAG Library routine E01ACF [13]). Contour plots were drawn using the larger table using the SIMPLEPLOT Mark I graphics package. All of the neutral stability curves presented above were produced in a similar way. In general, the contour plots obtained were smooth, but some of those for the unheated case did have slight ripples which were smoothed on the final versions of the figures. The interpolation program was also used to determine the minimum critical Reynolds number below which all

disturbances are stable. The values for various cases are in Table IX below. They are discussed further in Section 3.

Wall Temperature (°C)	Reynolds Number R	Number of Integration steps	Wavenumber $\bar{\alpha}$ Real	Wavenumber $\bar{\alpha}$ Imag	Frequency $\bar{\omega}$
32.2222	400	3200	0.05	0.024346	0.016689
		1600		0.024346	0.016689
		800		0.024346	0.016689
		400		0.024347	0.016689
	2000	3200	0.10	0.012078	0.025248
		1600		0.012078	0.025248
		800		0.012081	0.025246
		400		0.012109	0.025215
	20000	3200	0.15	-0.002720	0.026628
		1600		-0.002769	0.026617
		800		-0.003512	0.026507
		400		-0.011928	0.026425
65.5556	400	3200	0.05	0.032698	0.020750
		1600		0.032698	0.020750
		800		0.032698	0.020750
		400		0.032705	0.020750
	2000	3200	0.10	0.020908	0.022470
		1600		0.020908	0.022470
		800		0.020917	0.022465
		400		0.020998	0.022398
	20000	3200	0.15	-0.002655	0.022820
		1600		-0.002744	0.022794
		800		-0.004294	0.022565
		400		-0.020114	0.023288
93.3333	400	3200	0.05	0.048665	0.017552
		1600		0.048665	0.017552
		800		0.048666	0.017552
		400		0.048691	0.017553
	2000	3200	0.10	0.021585	0.020538
		1600		0.021587	0.020538
		800		0.021613	0.020525
		400		0.021804	0.020348
	20000	3200	0.15	-0.004155	0.021116
		1600		-0.004436	0.021047
		800		-0.009386	0.020606
		400		-0.028066	0.024785

Table VII Effect of number of integration steps on heated flat-plate eigenvalues

Wall Temperature (°C)	Fluid Properties/ Mean flow	Reynolds Number R	Wave Number, $\bar{\alpha}$ Real	Imag	Frequency $\bar{\omega}$
32.2222	Lowell/2nd order	400	0.05	0.024367	0.016687
	Lowell/4th order			0.024346	0.016689
(800 int	Lowell (const ρ)			0.024339	0.016688
steps)	Kaups & Smith			0.024297	0.016698
32.2222	Lowell/2nd order	2000	0.10	0.012070	0.025247
	Lowell/4th order			0.012081	0.025246
	Lowell (const ρ)			0.012086	0.025248
	Kaups & Smith			0.012122	0.025255
32.2222	Lowell/2nd order	20000	0.15	-0.003488	0.026511
	Lowell/4th order			-0.003511	0.026507
	Lowell (const ρ)			-0.003504	0.026506
	Kaups & Smith			-0.003488	0.026500
65.5556	Lowell/2nd order	400	0.05	0.032621	0.020642
	Lowell/4th order			0.032698	0.020750
(1600 int	Lowell (const ρ)			0.032690	0.020766
steps)	Kaups & Smith			0.032807	0.020832
65.5556	Lowell/2nd order	2000	0.10	0.020859	0.022467
	Lowell/4th order			0.020909	0.022470
	Lowell (const ρ)			0.020923	0.022467
	Kaups & Smith			0.020932	0.022464
65.5556	Lowell/2nd order	20000	0.15	-0.002712	0.022797
	Lowell/4th order			-0.002744	0.022794
	Lowell (const ρ)			-0.002750	0.022793
	Kaups & Smith			-0.002782	0.022797
93.3333	Lowell/2nd order	400	0.05	0.048365	0.017528
	Lowell/4th order			0.048665	0.017552
(1600 int	Lowell (const ρ)			0.048747	0.017540
steps)	Kaups & Smith			0.048943	0.017527
93.3333	Lowell/2nd order	2000	0.10	0.021542	0.020533
	Lowell/4th order			0.021587	0.020538
	Lowell (const ρ)			0.021574	0.020532
	Kaups & Smith			0.021520	0.020537
93.3333	Lowell/2nd order	20000	0.15	-0.002663	0.028493
	Lowell/4th order			-0.004436	0.021047
	Lowell (const ρ)			-0.004461	0.021047
	Kaups & Smith			-0.004547	0.021072

Table VIII The effect of different fluid property relations and different mean flows on heated flat-plate eigenvalues

Wall Temperature (°C)	Number of Integration Steps	Fluid Properties	Mean-flow Calculation	Minimum critical Reynolds number
15.5556	800		2nd order	521
			4th order	519
32.2222	800	Lowell	2nd order	5142
		Lowell	4th order	5136
		Lowell (const ρ)		5147
		Kaups & Smith		5199
65.5556	1600	Lowell	2nd order	11345
		Lowell	4th order	11297
		Lowell (const ρ)		11289
		Kaups & Smith		11227
93.3333	1600	Lowell	2nd order	8340
		Lowell	4th order	8281
		Lowell (const ρ)		8240
		Kaups & Smith		8101

Table IX *Effect of different fluid properties and different mean flows on minimum critical Reynolds number*

A few numerical results were obtained for the temporal stability case (mode 0) using the sixth-order program BMTST6 and these are compared with the corresponding fourth-order results in Table X. The wall temperature was 32.2°C (90°F), the freestream boundary at $\eta = 10$ and the Lowell fluid-property relations were used with 800 integration steps. In general, the results show a non-trivial but small difference between the fourth-order and sixth-order approaches. Neutral stability curves (which are the same for temporal and spatial instability) are compared in Figure 15, which shows that the differences between the two cases is the same as that obtained by Lowell.

Reynolds Number R	Wave Number $\bar{\alpha}$	Fourth-order Frequency, $\bar{\omega}$ Real	Imag	Sixth-order Frequency, $\bar{\omega}$ Real	Imag
5000	0.12000	0.026885	-0.000573	0.026820	-0.000705
6000	0.16000	0.037071	0.000190	0.036080	0.000138
7000	0.12233	0.025799	0.000080	0.025788	0.000003
8950	0.10668	0.021016	0.000074	0.021014	0.000002
14250	0.17315	0.033227	0.000081	0.033332	0.000000
400	0.05000	0.015543	-0.007361	0.015300	-0.006302
2000	0.10000	0.025579	-0.003712	0.024762	-0.004312
10000	0.15000	0.030417	0.000640	0.030477	0.000591
20000	0.15000	0.026593	0.000683	0.026732	0.000524

Table X Comparison of eigenvalues using fourth-order and sixth-order approaches

END

DATE
FILMED

7-87